Biodistribution and Radiation Dosimetry of the Anti-HER2 Affibody Molecule ^{68}Ga-ABY-025 in Breast Cancer Patients

Mattias Sandström[1], Karolina Lindskog[1], Irina Velikyan[1], Anders Wennborg[2], Joachim Feldwisch[2,3], Dan Sandberg[1], Vladimir Tolmachev[3], Anna Orlova[3], Jens Sörensen[1], Jörgen Carlsson[3], Henrik Lindman[4], and Mark Lubberink[1]

[1]Nuclear Medicine and PET, Department of Surgical Sciences, Uppsala University, Uppsala, Sweden; [2]Affibody AB, Solna, Sweden; [3]Biomedical Radiation Sciences, Rudbeck Laboratory, Department of Immunology, Genetics, and Pathology, Uppsala University, Uppsala, Sweden; and [4]Section of Oncology, Department of Immunology, Genetics, and Pathology, Uppsala, Sweden

^{68}Ga-ABY-025 is a radiolabeled Affibody molecule for in vivo diagnosis of human epidermal growth factor receptor 2 (HER2)–positive breast cancer tumors with PET. The aim of the present work was to measure the biodistribution and estimate the radiation dosimetry of ^{68}Ga-ABY-025 for 2 different peptide mass doses in a single group of patients using dynamic and serial whole-body PET/CT. **Methods:** Eight patients with metastatic breast cancer were included. Each patient underwent an abdominal 45-min dynamic and 3 whole-body PET/CT scans at 1, 2, and 4 h after injection of a low peptide dose (LD) and a high peptide dose (HD), with approximately the same amount of radioactivity, in separate investigations 1 wk apart. As input to the absorbed dose calculations, volumes of interest were drawn on all clearly identifiable source organs: liver, kidneys, spleen, descending aorta, and upper large intestine. Absorbed doses were calculated using OLINDA/EXM, version 1.1. **Results:** Of the major organs, the highest radionuclide uptake at 1, 2, and 4 h after injection was observed in the kidneys and liver. The highest absorbed organ doses were seen in the kidneys, followed by the liver for both LD and HD ^{68}Ga-ABY-025. Absorbed doses to liver and kidneys were slightly but significantly higher for LD. Total effective dose was 0.030 ± 0.003 mSv/MBq for LD and 0.028 ± 0.002 mSv/MBq for HD. **Conclusion:** The effective dose for a typical 200-MBq administration of ^{68}Ga-ABY-025 is 6.0 mSv for LD and 5.6 mSv for HD. Therefore, from a radiation dosimetry point of view, HD is preferred for PET/CT evaluation of HER2-expressing breast cancer tumors. These effective doses are somewhat higher than earlier published values for other ^{68}Ga-labeled tracers, such as 0.021 ± 0.003 mSv/MBq for ^{68}Ga-DOTATATE and ^{68}Ga-DOTATOC, mainly because of higher uptake in liver and kidney.

Key Words: Affibody; breast cancer metastases; dosimetry; HER2-receptor; ^{68}Ga-gallium

J Nucl Med 2016; 57:867–871
DOI: 10.2967/jnumed.115.169342

For women, breast cancer is currently the most common cancer. Human epidermal growth factor receptor 2 (HER2) is overexpressed in about 1 of 6 cases (*1–3*) at initial diagnosis and is associated with poor survival (*1,3*). Treatments targeted to HER2, such as with the anti-HER2 antibody trastuzumab, have considerably improved overall survival (*1,3,4*). Today, assessment of HER2 status is based on tumor biopsy. However, HER2 expression can vary between the primary tumor and metastases in up to 40% of cases (*2,5,6*) and metastatic HER2 expression can change over time, which could necessitate a change of therapy (*7,8*). Follow-up using biopsies cannot always be performed due to practical reasons or patient discomfort.

Molecular imaging using SPECT and PET might be a noninvasive, whole-body–based way to evaluate HER2 expression quantitatively. One such approach is the use of trastuzumab labeled with ^{111}In (half-time, 2.8 d) (*9*) or ^{89}Zr (3.3 d) (*10*) for use with SPECT and PET, respectively, but the slow kinetics of antibodies require imaging several days after administration. One promising method of fast, safe, and accurate imaging that specifically binds to a site on the receptor not occupied by current targeting therapeutic drugs (*11–13*) is to use the Affibody (Affibody AB) molecule ABY-025. ABY-025 labeled with ^{111}In used with SPECT has shown promising clinical results (*14*) that might be further improved when semiquantitative SUV SPECT becomes available. The use of PET and ABY-025 labeled with ^{68}Ga (half-time, 68 min) has the potential to provide higher-sensitivity, higher-resolution images with lower absorbed and effective doses. The use of a short-lived positron emitter, combined with the higher sensitivity of PET and the much faster kinetics of ABY-025 than of trastuzumab, will allow for imaging of the tumors within hours after injection instead of days, improving patient comfort and logistics. Tumor-to-background ratio, and hence detectability of tumors, may be dependent on the total amount of peptide injected, since the number of occupation sites may be much higher in tumor sites. Hence, the target receptors in normal organs can be saturated whereas the receptors in tumors are not. A preclinical study has previously indicated that it is possible to discriminate between low and high HER2 expression using Affibody molecules with low specific radioactivity (*15*). Such discrimination has also been indicated in a clinical (*14*) and a preclinical study (*16*) considering the fast clearance of radioactivity from low HER2-expressing tumors.

^{68}Ga-ABY-025 and PET have, in a recent study, been shown capable of discriminating HER2-positive metastases, with SUV correlating well with HER2 expression (*17*). In that study, 2 different amounts of peptides were administered, with the higher peptide dose giving the best results in terms of detectability and discrimination. The aim of the present work was to measure the biodistribution and estimate the radiation dosimetry of ^{68}Ga-ABY-025 in a single group of patients injected with 2 different peptide doses, but

Received Nov. 9, 2015; revision accepted Jan. 21, 2016.
For correspondence or reprints contact: Mattias Sandström, Medical Physics, Uppsala University Hospital, SE-75185, Uppsala, Sweden.
E-mail: mattias.sandstrom@akademiska.se
Published online Feb. 9, 2016.

approximately the same amount of radioactivity, using dynamic and serial whole-body PET/CT.

MATERIALS AND METHODS

Patients

Eight women diagnosed with metastatic breast cancer were included in the present work. The study was an academically sponsored clinical trial (trial identifiers EudraCT 2012-005228-14 and NCT01858116) approved by the Regional Board of Medical Ethics and the Swedish Medical Products Agency. All patients signed an informed consent form before inclusion in the study.

Radiochemistry

^{68}Ga-ABY-025 was produced in compliance with good manufacturing practices (*18*) using a fractionation method (*19*). ^{68}Ga was obtained from a ^{68}Ge/^{68}Ga-generator (IGG100; Eckert and Ziegler). ^{68}Ga-ABY-025 was prepared in 2 peptide doses (low [LD], 78 ± 8 μg, and high [HD], 427 ± 19 μg) with amounts of radioactivity in the same range, hence resulting in an approximately 6-fold difference in specific radioactivity values.

PET Protocol

PET data were acquired using a Discovery ST (GE Healthcare) PET/CT scanner. After a low-dose CT scan for patient positioning and attenuation correction, a 45-min dynamic PET scan (6 × 10, 4 × 60, 5 × 180, 5 × 300 s) over the abdominal region was started simultaneously with intravenous injection of 215 ± 58 MBq (range, 124–294 MBq) of LD ^{68}Ga-ABY-025. This was followed by 3 whole-body scans (proximal femur to base of skull) starting at 1, 2, and 4 h after injection, with scan durations of 3, 4, and 5 min per bed position, respectively, each preceded by a low-dose CT examination. Images were reconstructed using normalization and attenuation-weighted ordered-subsets expectation maximization (2 iterations, 21 subsets) including all appropriate corrections and a 5.4-mm gaussian postprocessing filter. Venous blood samples were drawn after each whole-body scan for measurement of whole-blood radioactivity concentrations. Patients were allowed to urinate between the dynamic scan and each consecutive whole-body scan. The urine was collected and weighed, and the radioactivity concentration was measured. Accurate cross-calibration between the PET/CT scanner, the dose calibrator, and the well counters used to measure blood and urine activity was verified monthly and was always within 3%. The scan procedure was repeated 1 wk later using 241 ± 49 MBq (range, 159–297 MBq) of HD ^{68}Ga-ABY-025.

Volumes of Interest

Volumes of interest were drawn on the whole-body images and in the last time frame of the dynamic image series over subsets of all clearly identifiable source organs: liver, kidneys, spleen, and upper large intestine. Volumes of interest drawn in the last frame of the dynamic scans were transferred to all earlier time frames. In addition, 70% isocontour regions of interest were drawn over 10 planes in first-pass images of the descending aorta, combined to a volume of interest, and transferred to all later dynamic time frames. Activity concentration and SUV normalized to body mass and injected amount of radioactivity were determined using the mean activity concentration in the volumes of interest. From these data, time–activity curves for these organs were computed. A whole-blood time–activity curve was computed by combining the descending aorta time–activity curve based on the dynamic scan with venous blood sample data taken after each whole-body scan.

Absorbed Dose Calculations

As in peptide receptor radionuclide therapy with ^{177}Lu-octreotate (*20*), the red marrow radioactivity concentration was assumed to equal the blood radioactivity concentration. Total organ activity was calculated by multiplying the radioactivity concentrations by the organ weights of the adult reference female phantom (*21*) scaled by the total patient weight. Urinary bladder contents were estimated on the basis of linear interpolation between decay-corrected measured amounts of excreted radioactivity, assuming complete voiding. After the last scan, a 4-h voiding interval with filling rates equivalent to those before the last measured urine sample was assumed. Time-integrated activity curves of the organ were calculated by trapezoidal integration until the last scan, followed by a single-exponential fit to the last 3 data points extrapolated to infinity. Residence times were obtained by dividing the time-integrated activity by the injected amount of activity. Small-intestine, upper-large-intestine, and lower-large-intestine residence times were estimated using gastrointestinal tract model 30 of the International Commission on Radiological Protection (*22*) based on the measured uptake in the upper large intestine. Activity in the remainder of the body was calculated as the injected activity minus the sum of the activity in all source organs and the activity excreted to urine up to each measurement point. Absorbed doses were calculated using OLINDA/EXM 1.1 (*23*).

Statistical Analysis

Differences between residence times and absorbed doses for both peptide masses were assessed using the Wilcoxon signed-rank test included in GraphPad Prism (version 6.02) software.

RESULTS

Figure 1 shows typical whole-body images of a single patient for both peptide masses with clear reduction of hepatic radioactivity uptake for the HD. Figure 2 shows the biodistribution, in terms of SUV and percentage injected activity per organ, for LD and HD. Of the major organs, the highest SUV at 60–240 min after injection was observed in the kidney, followed by liver. Figure 3 directly compares the SUV in kidney and liver for LD versus HD. Initial uptake in the liver was higher for LD, whereas clearance appeared similar for LD and HD, resulting in a higher residence time ($P < 0.05$). For the kidney, a smaller difference in the same direction was found, whereas blood clearance was faster for LD. Residence times, as shown in Table 1, considering mean data from the 8 patients, were highest for liver, followed by kidneys.

Absorbed dose estimates are shown in Table 2. The highest absorbed organ doses

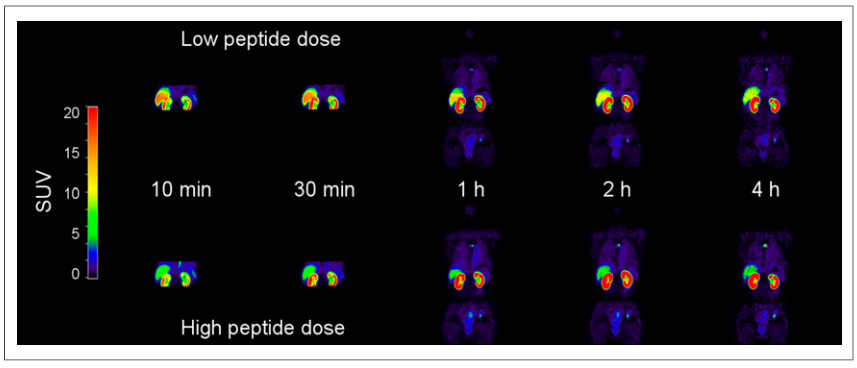

FIGURE 1. Representative whole-body images at 10, 30, 60, 120, and 240 min after injection of LD and HD in same patient.

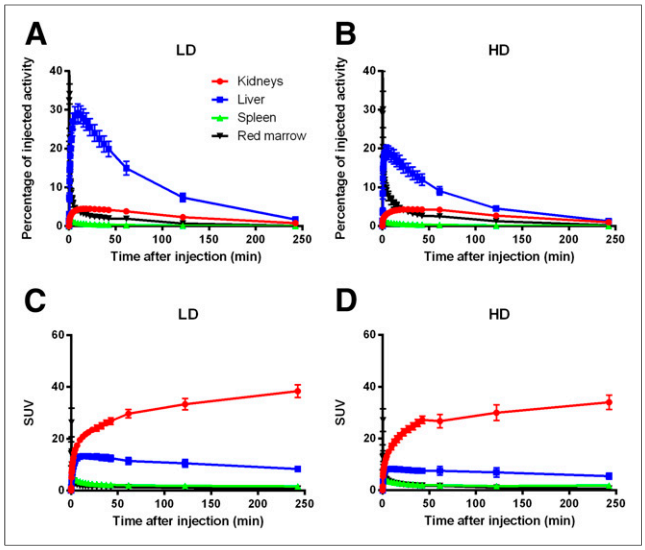

FIGURE 2. Percentage injected activity (A and B) and SUV (C and D) as function of time after injection in kidneys, liver, spleen, and red marrow for LD (A and C) and HD (B and D). Error bars indicate SD. Percentage of injected radioactivity was not corrected for radioactive decay.

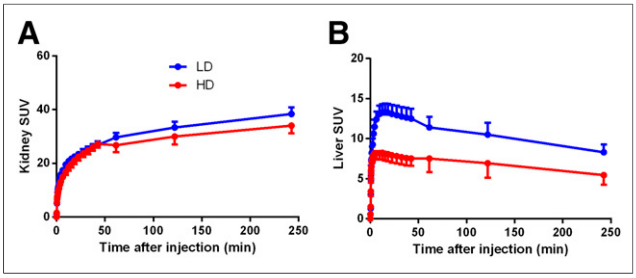

FIGURE 3. Direct comparison of SUV in kidney (A) and liver (B) for LD vs. HD. Error bars indicate SD.

TABLE 1
Residence Times

Site	LD	HD
Kidney*	0.238 ± 0.029	0.216 ± 0.047
Liver*	0.456 ± 0.135	0.366 ± 0.144
Spleen	0.010 ± 0.003	0.009 ± 0.002
Urinary bladder contents	0.004 ± 0.002	0.005 ± 0.002
Bone marrow*	0.028 ± 0.010	0.038 ± 0.014
Heart contents*	0.009 ± 0.003	0.012 ± 0.005
Small intestine contents	0.007 ± 0.002	0.006 ± 0.002
Upper large intestine contents	0.002 ± 0.001	0.002 ± 0.001
Lower large intestine contents	0.000 ± 0.000	0.000 ± 0.000
Remainder of body*	0.871 ± 0.140	0.971 ± 0.167

*Significant difference between peptide masses LD and HD (Wilcoxon signed-rank test; $P < 0.05$).
Data are mean hours ± SD ($n = 8$).

were seen in kidney and liver. Figure 4 compares residence times and absorbed doses in kidney and liver, as well as effective dose, for each individual patient.

Total effective dose was 0.030 ± 0.002 mSv/MBq for LD and 0.028 ± 0.003 mSv/MBq for HD. These values would result in an effective dose of 6.0 and 5.6 mSv for a typical administration of about 200 MBq as used in the present study.

Absorbed doses to kidney, liver, gallbladder wall, and total body were significantly higher for LD, whereas red marrow absorbed dose was significantly higher for HD (Wilcoxon test, $P < 0.05$), although mean absolute differences were very small for gallbladder wall (1%), total body (2%), and red marrow (2%).

DISCUSSION

To our knowledge, the present work is the first study of the radiation dosimetry of ^{68}Ga-ABY-025. Absorbed radiation doses were estimated using a protocol combining dynamic PET and serial whole-body PET scans in 8 evaluable patients. An effective

TABLE 2
^{68}Ga-ABY-025 Absorbed Doses

Site	LD	HD
Adrenals	0.022 ± 0.001	0.021 ± 0.001
Brain	0.009 ± 0.001	0.010 ± 0.002
Breasts	0.010 ± 0.001	0.011 ± 0.001
Gallbladder wall*	0.023 ± 0.002	0.022 ± 0.002
Lower large intestine wall	0.012 ± 0.002	0.013 ± 0.002
Small intestine	0.017 ± 0.002	0.017 ± 0.001
Stomach wall	0.015 ± 0.003	0.015 ± 0.001
Upper large intestine wall	0.017 ± 0.001	0.017 ± 0.001
Heart wall*	0.019 ± 0.003	0.022 ± 0.004
Kidney*	0.404 ± 0.049	0.366 ± 0.079
Liver*	0.170 ± 0.049	0.137 ± 0.052
Lungs	0.013 ± 0.001	0.014 ± 0.001
Muscle	0.011 ± 0.001	0.012 ± 0.001
Ovaries	0.012 ± 0.001	0.013 ± 0.002
Pancreas	0.019 ± 0.000	0.019 ± 0.000
Red marrow*	0.015 ± 0.002	0.017 ± 0.003
Osteogenic cells	0.021 ± 0.003	0.023 ± 0.004
Skin	0.009 ± 0.001	0.010 ± 0.001
Spleen	0.039 ± 0.008	0.037 ± 0.006
Thymus	0.011 ± 0.001	0.012 ± 0.002
Thyroid	0.010 ± 0.001	0.011 ± 0.002
Urinary bladder wall	0.016 ± 0.004	0.018 ± 0.003
Uterus	0.012 ± 0.001	0.013 ± 0.002
Total body*	0.018 ± 0.000	0.018 ± 0.000
Effective dose equivalent (mSv/MBq)	0.048 ± 0.004	0.045 ± 0.006
Effective dose (mSv/MBq)	0.030 ± 0.002	0.028 ± 0.003

*Significant difference between peptide masses LD and HD (Wilcoxon signed-rank test; $P < 0.05$).
Data are mean mGy/MBq ± SD ($n = 8$).

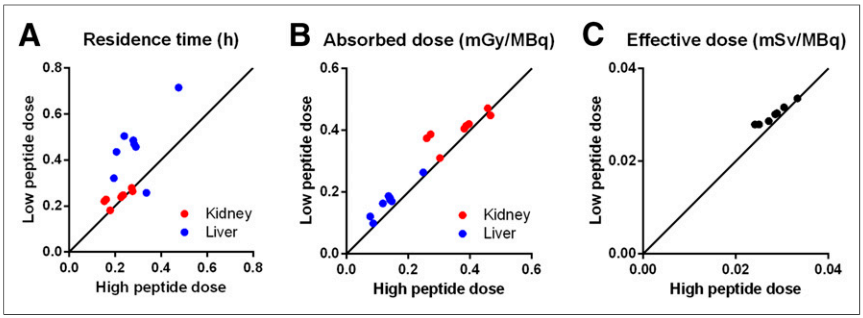

FIGURE 4. Residence times (A), absorbed doses in kidney and liver (B), and effective dose (C) for each patient, shown as LD vs. HD. Solid line in each panel is line of identity between LD and HD.

dose of 3.0 mSv and 2.8 mSv for LD and HD, respectively, will be achieved for a 100-MBq administration, which may be sufficient for clinical use. The administration of about 200 MBq, as in the present study, would give an effective dose in the range of 5–6 mSv. These values are considerably lower than the effective dose of 21 mSv calculated for the administration of 200 MBq of ^{111}In-ABY-025 in a previous investigation (*14*) and also lower than for typical ^{18}F-FDG PET examinations, which often give effective doses of around 7 mSv. However, these dose estimates are higher than the earlier published values of 0.021 ± 0.003 for ^{68}Ga-DOTATATE and ^{68}Ga-DOTATOC because of higher uptake in liver and kidney. Another positron-emitting radiometal that has been used to label larger molecules is ^{89}Zr. However, the use of ^{89}Zr is preferred mainly for tracers with slow kinetics, such as antibodies, because of its long radioactive half-life (3.3 d). This longer half-life inherently results in higher effective doses, such as 0.55 ± 0.07 mSv/MBq for ^{89}Zr-ibritumomab tiuxetan (*24*). For the present patient group, the absorbed doses due to ^{68}Ga-ABY-025 should also be seen through the perspective that diagnostic CT scans of the thorax and abdomen will give comparable or higher effective doses. In addition, many patients will undergo radiation treatment, leading to much higher radiation doses.

The use of a combined dynamic–whole-body protocol allows for detailed assessment of the time–activity curves of predefined risk organs while improving patient comfort by allowing patients to leave the scanner between subsequent whole-body scans. The use of a 45-min dynamic scan has the disadvantage of not being able to follow other risk organs during this time. However, on the basis of earlier studies with this compound (*14*), it is well known that the main source and risk organs are the liver and the kidneys. Because both of these can be imaged in one bed position, the advantage of being able to image these organs over 45 min exceeded the disadvantage of not being able to image other risk organs during this time.

Absorbed doses in kidneys and liver were slightly higher for LD than for HD, and the same was observed for the effective dose. Differences in effective dose were minor even within individual patients. The organ receiving the highest absorbed radiation dose was the kidney, followed by the liver. The absorbed dose to these organs, after a 100-MBq administration, will be approximately 40 mGy and 15 mGy, respectively, which is less than the maximum allowed absorbed dose of 50 mGy to a single organ in a healthy adult research subject (*25*).

Because the scan protocol covered the major part of the radioactive decay of ^{68}Ga, the remainder of the decay after the last scan amounted to at most a small percentage of the total number of disintegrations in each organ. Therefore, the uncertainty in extrapolation after the 4-h whole-body scan had only minor effects on the total estimate of the time-integrated activity.

The patients in the present work had breast cancer tumors and metastases with varying degree of HER2 expression, and this factor is not accounted for in OLINDA/EXM 1.1 calculations to assess radiation dosimetry. However, the tumor burden was limited, and since the major part of the absorbed dose to the adrenal glands, kidneys, and healthy liver tissue was due to locally absorbed β-radiation, taking into account the cross dose from tumors to healthy tissues would have resulted in negligible changes in organ doses.

CONCLUSION

The effective dose for a typical 200-MBq administration of ^{68}Ga-ABY-025 was found to be 6.0 mSv for LD (78 ± 8 μg) and 5.6 mSv for HD (427 ± 19 μg) ^{68}Ga-ABY-025. The absorbed doses to kidneys and liver were lower for HD than for LD. Assuming that tumor uptake was unaffected by peptide dose, these results suggest a higher tumor-to-background contrast for HD. Therefore, in terms of biodistribution and dosimetry, HD is preferred in the diagnosis and pretreatment HER2-status evaluation of breast cancer patients.

DISCLOSURE

The costs of publication of this article were defrayed in part by the payment of page charges. Therefore, and solely to indicate this fact, this article is hereby marked "advertisement" in accordance with 18 USC section 1734. This work was sponsored by the Swedish Cancer Society (Cancerfonden) and the Swedish Breast Cancer Foundation (Bröstcancerfonden). Affibody AB donated the ABY-025. No other potential conflict of interest relevant to this article was reported.

ACKNOWLEDGMENTS

We thank Mimmi Lidholm, Annie Bjurebäck, Maj Wiberg, Lars Lindsjö, Mirtha Ponce Zoto, and Marie Åhlman for their technical assistance in performing the scans.

REFERENCES

1. Cortés J, Fumoleau P, Bianchi GV, et al. Pertuzumab monotherapy after trastuzumab-based treatment and subsequent reintroduction of trastuzumab: activity and tolerability in patients with advanced human epidermal growth factor receptor 2-positive breast cancer. *J Clin Oncol.* 2012;30:1594–1600.
2. Houssami N, Macaskill P, Balleine RL, Bilous M, Pegram MD. HER2 discordance between primary breast cancer and its paired metastasis: tumor biology or test artefact? Insights through meta-analysis. *Breast Cancer Res Treat.* 2011;129:659–674.
3. Verma S, Miles D, Gianni L, et al. Trastuzumab emtansine for HER2-positive advanced breast cancer. *N Engl J Med.* 2012;367:1783–1791.
4. Slamon DJ, Leyland-Jones B, Shak S, et al. Use of chemotherapy plus a monoclonal antibody against HER2 for metastatic breast cancer that overexpresses HER2. *N Engl J Med.* 2001;344:783–792.

5. Aurilio G, Disalvatore D, Pruneri G, et al. A meta-analysis of oestrogen receptor, progesterone receptor and human epidermal growth factor receptor 2 discordance between primary breast cancer and metastases. *Eur J Cancer.* 2014;50:277–289.
6. Wilking U, Karlsson E, Skoog L, et al. HER2 status in a population-derived breast cancer cohort: discordances during tumor progression. *Breast Cancer Res Treat.* 2011;125:553–561.
7. Karlsson E, Sandelin K, Appelgren J, et al. Clonal alteration of breast cancer receptors between primary ductal carcinoma in situ (DCIS) and corresponding local events. *Eur J Cancer.* 2014;50:517–524.
8. Lindström LS, Karlsson E, Wilking UM, et al. Clinically used breast cancer markers such as estrogen receptor, progesterone receptor, and human epidermal growth factor receptor 2 are unstable throughout tumor progression. *J Clin Oncol.* 2012;30:2601–2608.
9. Gaykema SB, de Jong JR, Perik PJ, et al. ^{111}In-trastuzumab scintigraphy in HER2-positive metastatic breast cancer patients remains feasible during trastuzumab treatment. *Mol Imaging.* 2014;13.
10. Dijkers EC, Oude Munnink TH, Kosterink JG, et al. Biodistribution of ^{89}Zr-trastuzumab and PET imaging of HER2-positive lesions in patients with metastatic breast cancer. *Clin Pharmacol Ther.* 2010;87:586–592.
11. Ahlgren S, Orlova A, Wallberg H, et al. Targeting of HER2-expressing tumors using ^{111}In-ABY-025, a second-generation affibody molecule with a fundamentally reengineered scaffold. *J Nucl Med.* 2010;51:1131–1138.
12. Eigenbrot C, Ultsch M, Dubnovitsky A, Abrahmsen L, Hard T. Structural basis for high-affinity HER2 receptor binding by an engineered protein. *Proc Natl Acad Sci USA.* 2010;107:15039–15044.
13. Feldwisch J, Tolmachev V, Lendel C, et al. Design of an optimized scaffold for affibody molecules. *J Mol Biol.* 2010;398:232–247.
14. Sörensen J, Sandberg D, Sandstrom M, et al. First-in-human molecular imaging of HER2 expression in breast cancer metastases using the ^{111}In-ABY-025 affibody molecule. *J Nucl Med.* 2014;55:730–735.
15. Tolmachev V, Wallberg H, Sandstrom M, Hansson M, Wennborg A, Orlova A. Optimal specific radioactivity of anti-HER2 Affibody molecules enables discrimination between xenografts with high and low HER2 expression levels. *Eur J Nucl Med Mol Imaging.* 2011;38:531–539.
16. Tolmachev V, Tran TA, Rosik D, Sjoberg A, Abrahmsen L, Orlova A. Tumor targeting using Affibody molecules: interplay of affinity, target expression level, and binding site composition. *J Nucl Med.* 2012;53: 953–960.
17. Sörensen J, Velikyan I, Sandberg D, et al. Measuring HER2-receptor expression in metastatic breast cancer using [^{68}Ga]ABY-025 Affibody PET/CT. *Theranostics.* 2016;6:262–271.
18. Velikyan I, Wennborg A, Feldwisch J, et al. GMP compliant preparation of a ^{68}gallium-labeled Affibody analogue for breast cancer patient examination: first-in-man. *Eur J Nucl Med Mol Imaging.* 2014;41(suppl):S228–S229.
19. Velikyan I, Beyer GJ, Langstrom B. Microwave-supported preparation of ^{68}Ga bioconjugates with high specific radioactivity. *Bioconjug Chem.* 2004;15:554–560.
20. Forrer F, Krenning EP, Kooij PP, et al. Bone marrow dosimetry in peptide receptor radionuclide therapy with [^{177}Lu-DOTA^{0},Tyr^{3}]octreotate. *Eur J Nucl Med Mol Imaging.* 2009;36:1138–1146.
21. Stabin MG. MIRDOSE: personal computer software for internal dose assessment in nuclear medicine. *J Nucl Med.* 1996;37:538–546.
22. *ICRP Publication 30: Limits for Intakes of Radionuclides by Workers*. Ottawa, Ontario, Canada: International Commission on Radiological Protection; 1980.
23. Stabin MG, Sparks RB, Crowe E. OLINDA/EXM: the second-generation personal computer software for internal dose assessment in nuclear medicine. *J Nucl Med.* 2005;46:1023–1027.
24. Rizvi SN, Visser OJ, Vosjan MJ, et al. Biodistribution, radiation dosimetry and scouting of ^{90}Y-ibritumomab tiuxetan therapy in patients with relapsed B-cell non-Hodgkin's lymphoma using ^{89}Zr-ibritumomab tiuxetan and PET. *Eur J Nucl Med Mol Imaging.* 2012;39:512–520.
25. Title 21: Food and drugs. Chapter I: Food and Drug Administration Department of Health and Human Services. Subchapter D: Drugs for Human Use. Part 361: Prescription Drugs for Human Use Generally Recognized as Safe and Effective and Not Misbranded—Drugs Used in Research. U.S. Food and Drug Administration website. https://www.accessdata.fda.gov/scripts/cdrh/cfdocs/cfcfr/CFRSearch.cfm?CFRPart=361&showFR=1. Accessed February 25, 2016.